Electronic Supplementary Information

Low-cost synthesis of nanocomposite of MoS_2 and alkali-activated halloysite nanotubes for photocatalytic RhB degradation†

Dongxu Wang,[a,b] Jiaxuan Bai,[a,b] Ming Hao,[a,b] Jinsheng Liang[a,b] Baizeng Fang[c,*] Yulei Wang,[a,b] Kaibin Cui,[a,b] Fei Wang,[a,b,*]

[a] Key Laboratory of Special Functional Materials for Ecological Environment and Information (Hebei University of Technology), Ministry of Education, Tianjin, 300130, PR China. Email: wangfei@hebut.edu.cn (F. Wang).

[b] School of Materials Science and Engineering (Hebei University of Technology), Tianjin, 300130, PR China

[c] Department of Chemical and Biological Engineering, The University of British Columbia, Vancouver, V6T 1Z3, Canada. Email: baizengfang@163.com (B. Fang).

Experimental

Chemicals

HNTs powder was originated from Guangdong province of China. The sodium hydroxide (NaOH), ammonium molybdate ($(NH_4)_6Mo_7O_{24}\cdot 4H_2O$), thiourea ($CH_4N_2S$), and rhodamine B (RhB) were supplied by Kewei Chemical Group Co., Ltd. Deionized (DI) water was used in all experiments. All chemicals were used without further treatment.

Preparation of alkali-activated HNTs (a-HNTs)

2 g of the as-received HNTs was suspended in 100 mL of NaOH solution (5 M), and then the mixture was magnetically stirred for 24 h at room temperature. The solid was collected by centrifugation and washed several times with DI water until the pH of the filtrate reached 7. The a-HNTs were obtained after drying at 60 °C for 12 h.

Synthesis of the MoS_2/a-HNTs nanocomposite

The MoS_2/a-HNTs nanocomposite was fabricated by a hydrothermal method, as shown in Figure S1. Briefly, 0.56 g of a-HNTs was added in 70 mL of DI water and ultrasonicated for 20 min. Then, 2.47 g of $(NH_4)_6Mo_7O_{24}\cdot 4H_2O$ and 4.56 g of CH_4N_2S were dissolved into the above suspension under magnetic stirring for 30 min. After that, 50 mL of the mixed solution was transferred into 100 mL Teflon-lined stainless autoclave. The mixture was sealed and maintained at 220 °C for 24 h. After cooling to room temperature, the final black precipitate was collected by filtrating, washing, and drying to obtain the MoS_2/a-HNTs nanocomposite. The pure MoS_2 and MoS_2/HNTs were synthesized similar to the MoS_2/a-HNTs nanocomposite excepted for without adding a-HNTs or replacing a-HNTs with raw HNTs.

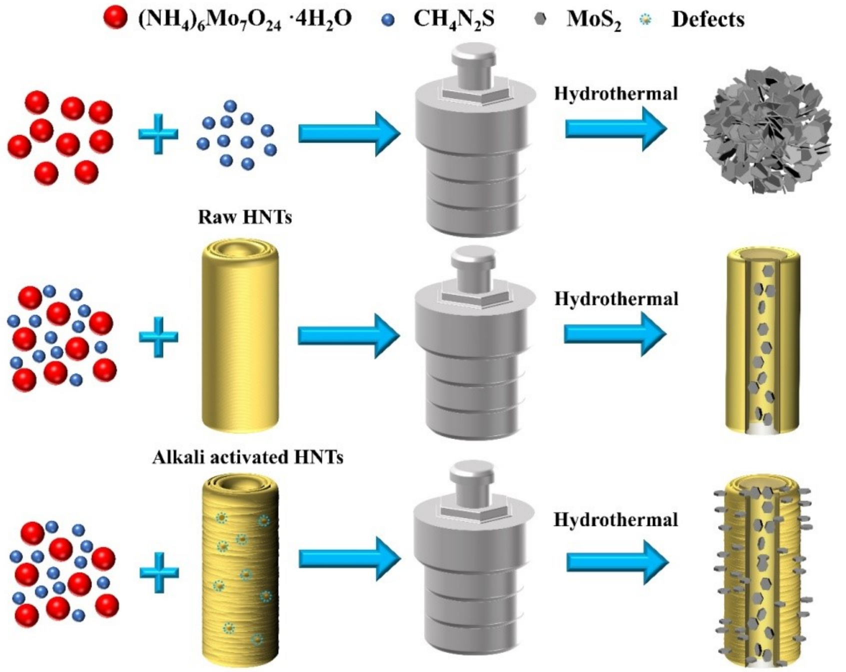

Fig. S1 Schematic diagram for the synthesis of pristine MoS_2 NSs (top), raw HNTs supported MoS_2 NSs (middle), and alkali-activated HNTs supported MoS_2 NSs (bottom).

Characterization

The as-synthesized samples were examined by X-ray powder diffraction (XRD), which was carried out on a Smart Lab 9 KW X-ray diffractometer with working conditions of Cu Kα radiation (λ = 1.54 Å), 40 mA, and 40 kV. Fourier-transform infrared spectroscopy (FT-IR) spectra of the samples were recorded in transmission mode from 400 to 4000 cm^{-1} on a Tensor II Fourier transform infrared spectrometer purchased from Bruker in Germany. The morphologies of the as-synthesized samples were observed by using a Quanta FEG450 scanning electron microscope (SEM) (FEI, USA) working at 30 kV. Transmission electron microscope (TEM), high-resolution

TEM (HRTEM), and energy-dispersive X-ray spectroscopy (EDS) were carried out by JEM 2100F transmission electron microscope from JEOL in Japan at an accelerating voltage of 200 kV. The N_2 adsorption-desorption tests were conducted on Autosorb-iQ2. All samples were outgassed in nitrogen flow at 200 °C for 4 h before measurements. The specific surface area (SSA) was evaluated using the Brunauer-Emmett-Teller (BET) method, and the total pore volume was calculated at the relative pressure of approximately 0.99. The pore size distribution was computed using the Barrett-Joyner-Halenda (BJH) method. The ultraviolet–visible (UV–vis) diffuse reflectance spectra (DRS) were obtained on U-3900H spectrophotometer (HITACHI) in the range of 240–800 nm using $BaSO_4$ as reference.

Photocatalytic tests

Photocatalytic activity of the as-prepared catalysts was assessed by the degradation of RhB in aqueous solutions, irradiated by a 500 W Xe lamp equipped with a cut-off filter ($\lambda > 420$ nm). In a typical evaluation procedure, 20 mg of catalyst was added into 100 mL of RhB solution (20 mg/L) at room temperature. The suspension solution was mixed under the vigorous stirring in dark for 0.5 h to reach the equilibrium of adsorption/desorption before visible light irradiation. At intervals of 0.5 h, 5.6 mL of the suspension was collected and centrifuged for subsequent absorbance analysis. The concentration of dye solution was analyzed by recording the UV-vis spectra using a Shimadzu UV-1800 spectrophotometer at wavelength of 553 nm. The degradation rate (%) was calculated according to the following formula: degradation rate (%) = $(A_0 - A_t)/A_0 \times 100\%$, where A_0 was the absorbance when adsorption/desorption equilibrium was achieved, and A_t was the absorbance after time t irradiation. To evaluate the effect of the main active species during photocatalysis, the scavengers including tert-butyl alcohol (TBA), ascorbic acid (AA), and ethylenediaminetetraacetic acid disodium salt (EDTA-2Na) were adopted for capturing hydroxyl radical ($\cdot OH$), superoxide radical ($\cdot O^{2-}$), and photogenerated hole (h^+), respectively.

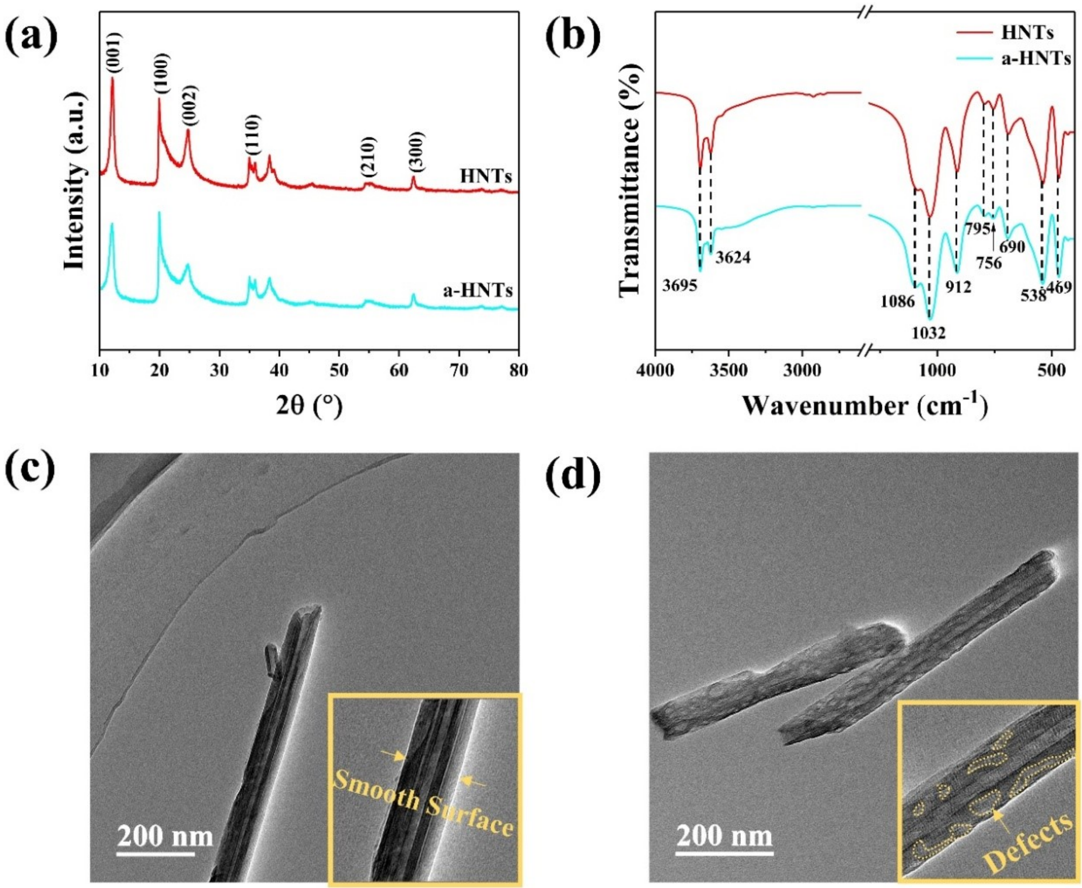

Fig. S2 Microstructure and morphology analysis of the raw HNTs and a-HNTs. (a) XRD pattern, (b) FT-IR spectra, and (c-d) TEM images of the raw HNTs and a-HNTs.

Notes on Fig. S2: The crystal structure, surface functional group, and morphology of raw HNTs and a-HNTs were systematically investigated at first. It could be seen that the HNTs retained their origin crystal structure after the alkali treatment, and 0.732 nm of d(001) indicated the dehydrated state of HNTs (JCPDS Card. No. 29-1487).[1] The weak peaks at 35.9° and 38.4° could be due to the minor impurities of kaolinite and dickite existed in HNTs.[2] It's worth noting that the intensity of (001) and (002) reflections of the HNTs decreased obviously after the alkali modification, indicating the decreased crystallinity for the a-HNTs. Meanwhile, the surface functional groups of HNTs almost unchanged as well after the alkali treatment (Fig. S2b†), including O-H stretching of the inner-surface hydroxyl groups and inner hydroxyl groups at 3695 and 3624 cm^{-1}, O-H deformation of inner Al-OH hydroxyl groups at 912 cm^{-1}, in-plane Si-O stretching at 1086 and 1032 cm^{-1}, symmetric Si-O-Si stretching at 795 cm^{-1}, and the perpendicular Si-O-Al stretching at 690 and 756 cm^{-1}.[3,4] A slight decrease of Si-O-Si deformation at 469 cm^{-1} was mainly because of the attack on the tetrahedral SiO_4 at outer surface of HNTs during alkali treatment.[5,6] Furthermore, the HNTs maintained the tube morphology while abundant defects were generated on the outer surface of the HNTs after the alkali activation, which was confirmed by TEM images (Figs. S2c and d). The generated defects could explain well the decreased crystallinity and intensity of Si-O-Si deformation for the a-HNTs. In addition, the alkali treatment also released the surface area of HNTs and more mesopores were produced (Fig. S3).

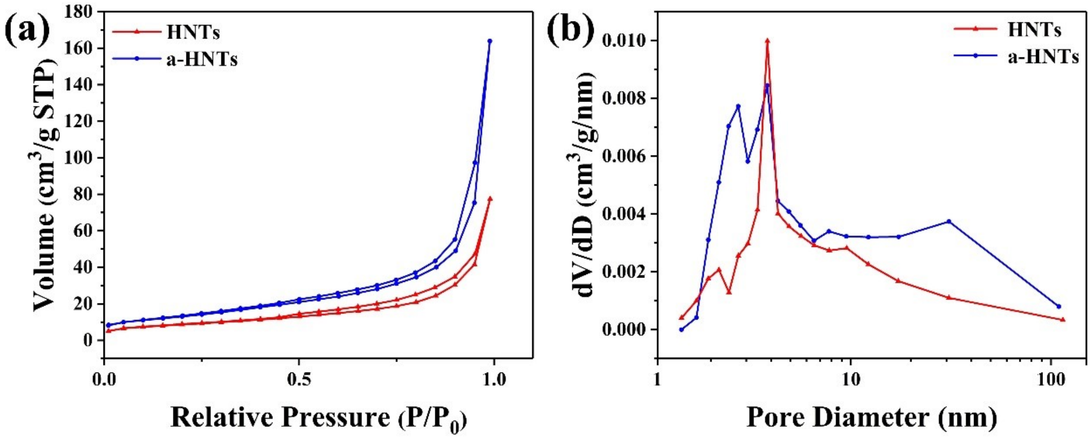

Fig. S3 (a) N_2 adsorption-desorption isotherms and (b) pore size distribution curves of raw HNTs and a-HNTs.

Notes on Fig. S3: The specific surface area (SSA) and pore size distribution (PSD) also played important roles for carrier. As shown in Fig. S3a, the isotherms of both samples could be classified as type IV with an H3 hysteresis loop, suggesting their mesoporous characteristic.[7] The SSA of raw HNTs was calculated to be 30.7 m^2/g while it increased to 46.5 m^2/g after the alkali treatment. Meanwhile, abundant pores with the average size of 2.5 nm for a-HNTs were newly generated (Fig. S3b†). Besides, a small amount of ~30 nm pores were also produced, which was probably due to the increased lumen size and decreased wall thickness according to previous study.[8-10] The pore volumes of HNTs also increased from 0.12 cm^3/g to 0.25 cm^3/g after the alkali activation.

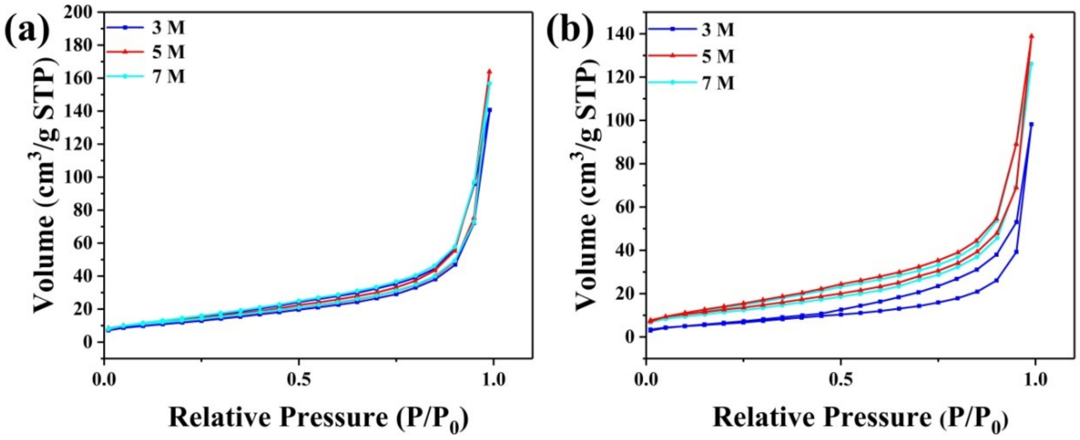

Fig. S4 N_2 adsorption-desorption isotherms of the HNTs modified by different NaOH concentrations (a), and the MoS_2/a-HNTs nanocomposite with HNTs modified by different NaOH concentrations (b).

Notes on Fig. S4: As the concentration of NaOH increased, the SSA of the HNTs also slightly increased (Fig. S4a). The SSA of HNTs modified by 3M, 5M, and 7M NaOH was determined to be ca. 43.5, 46.5 and 47.0 m^2/g respectively. Meanwhile, the MoS_2/a-HNTs nanocomposite with HNTs modified by 5M NaOH exhibited the largest SSA of ca. 45.4 m^2/g.

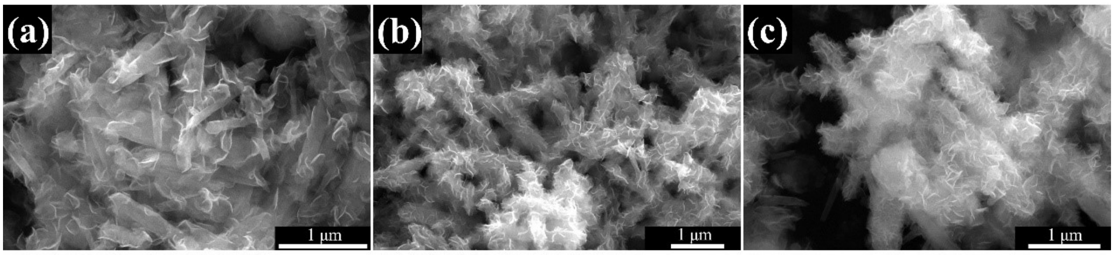

Fig. S5 SEM images of the MoS_2/a-HNTs nanocomposite with HNTs modified by 3M (a), 5M (b), and 7M (c) NaOH.

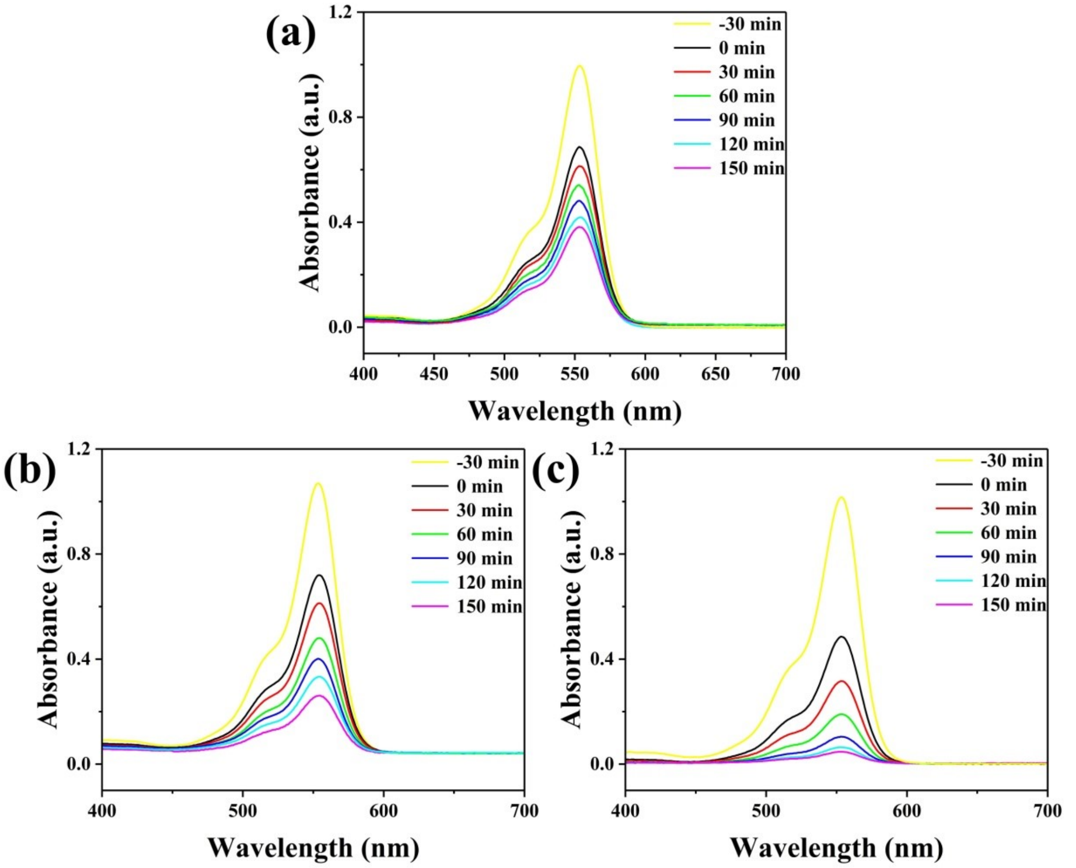

Fig. S6 Time dependent adsorption spectra variations of RhB at different degradation times recorded on the various materials: MoS_2 (a), MoS_2/HNTs (b), and MoS_2/a-HNTs (c).

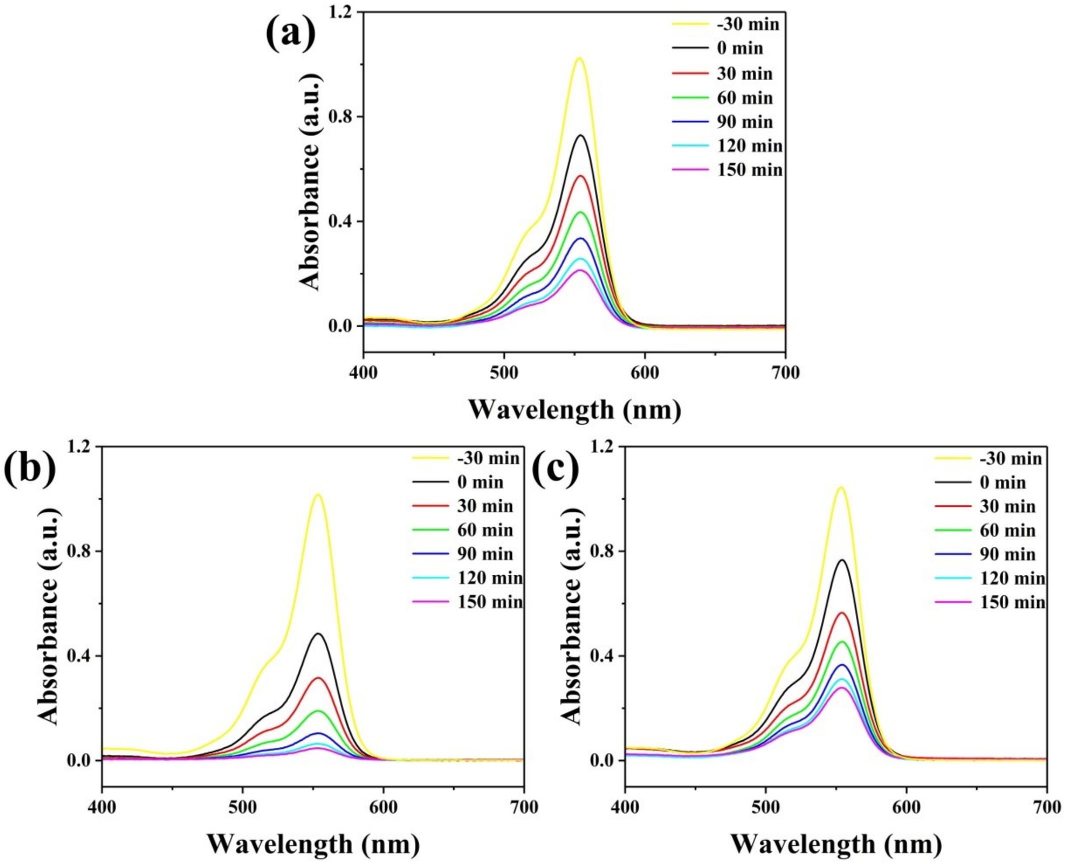

Fig. S7 Time dependent adsorption spectra variations of RhB at different degradation times in the presence of the MoS_2/a-HNTs nanocomposite with HNTs modified by 3M (a), 5M (b), and 7M (c) NaOH.

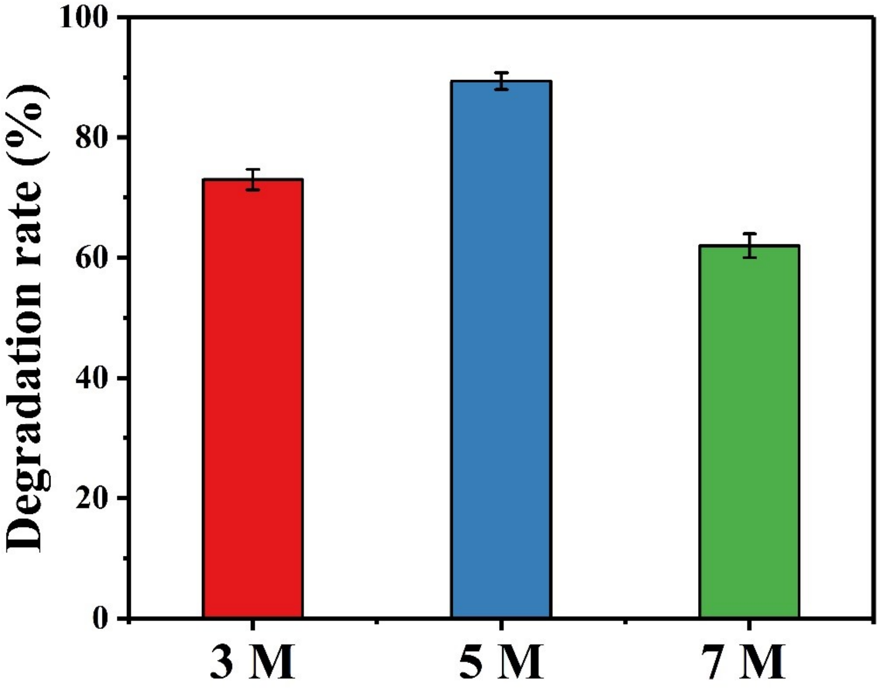

Fig. S8 The degradation rate of the MoS_2/a-HNTs nanocomposite with HNTs modified by different NaOH concentrations.

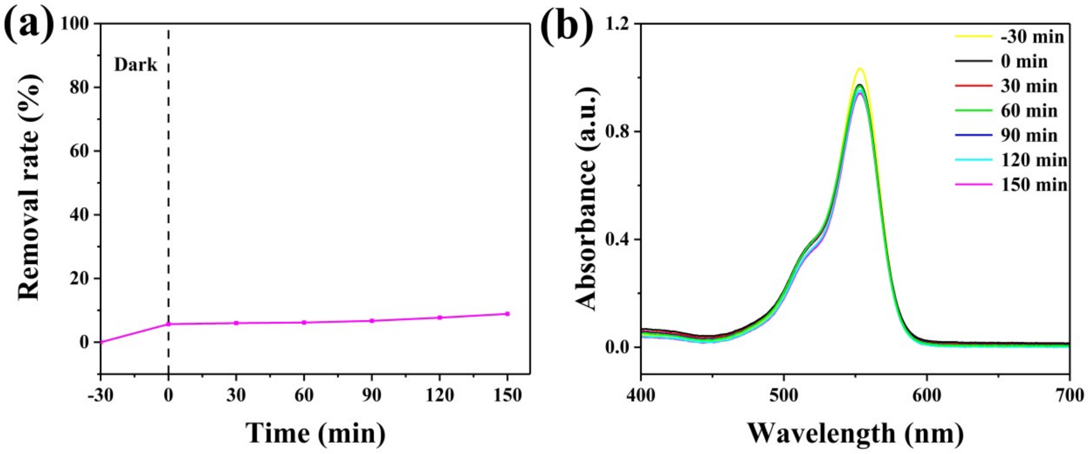

Fig. S9 (a) Removal efficiency of RhB by the a-HNTs and (b) time dependent adsorption spectra variations of RhB at different degradation times in the presence of the a-HNTs.

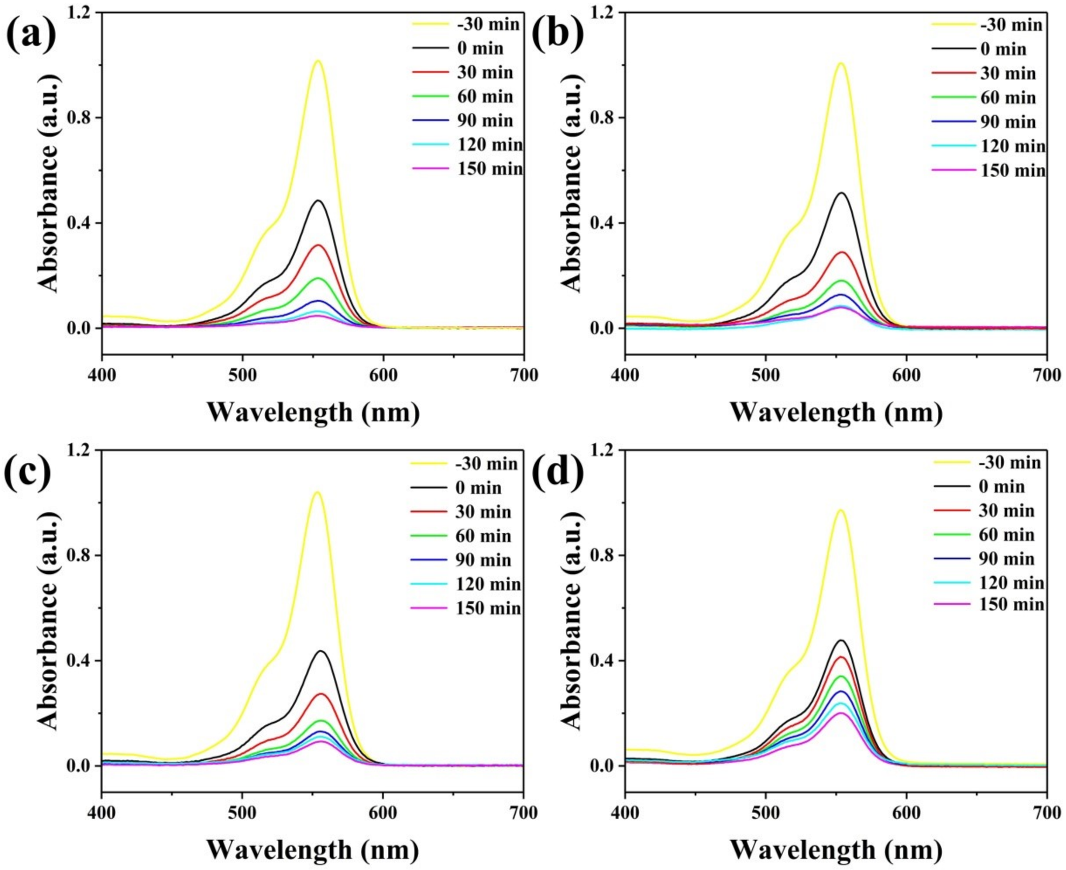

Fig. S10 Time dependent adsorption spectra variations of RhB at different degradation times during the radical trapping experiments by using: None (a), TBA (b), AA (c), and EDTA-2a (d).

References

1 E. Van Ranst, P. Kips, J. Mbogoni, F. Mees, M. Dumon and B. Delvaux, *Geoderma*, 2020, **375**, 114527.

2 B. Čalija, J. Milić, N. Milašinović, A. Daković, K. Trifković, J. Stojanović and D. Krajišnik, *J. Appl. Polym. Sci.*, 2019, **137**, 48406.

3 G. Fakhrullina, E. Khakimova, F. Akhatova, G. Lazzara, F. Parisi and R. Fakhrullin, *ACS Appl. Mater. Interfaces*, 2019, **11**, 23050-23064.

4 P. Sun, G. Liu, D. Lv, X. Dong, J. Wu and D. Wang, *J. Appl. Polym. Sci.*, 2016, **133**, 43249.

5 Y. Song, P. Yuan, P. Du, L. Deng, Y. Wei, D. Liu, X. Zhong and J. Zhou, *Appl. Clay Sci.*, 2020, **186**, 105450.

6 R. D. White, D. V. Bavykin and F. C. Walsh, *Nanotechnology*, 2012, **23**, 065705.

7 M. Thommes, K. Kaneko, A. V. Neimark, J. P. Olivier, F. Rodriguez-Reinoso, J. Rouquerol and K. S. W. Sing, *Pure Appl. Chem.*, 2015, **87**, 1051-1069.

8 Y. H. Ahmad, A. T. Mohamed and S. Y. Al-Qaradawi, *Appl. Clay Sci.*, 2021, **201**, 105956.

9 M. H. Lee, H. S. Seo and H. J. Park, *J. Food Sci.*, 2017, **82**, 922-932.

10 L. Li, H. Fan, L. Wang and Z. Jin, *RSC Adv.*, 2016, **6**, 54193-54201.